Structure and Properties of Drawn Tapes of High-Density Polyethylene/Ethylene-Propylene Copolymer Blends. II

S. J. MAHAJAN,[1] B. L. DEOPURA[1,*] and YIMIN WANG[2]

[1]Textile Technology Department, Indian Institute of Technology, New Delhi 110016, India, and
[2]Chemical Fibre Research Institute, China Textile University, Shanghai 200051, China

SYNOPSIS

A series of oriented tapes has been prepared from the blends consisting of high-density polyethylene (HDPE), with isotactic polypropylene (PP) and ethylene–propylene block copolymer (EP_bC). The mechanical properties and structure–morphology of blends were investigated using differential scanning calorimetry, polarizing microscopy, wide- and small-angle X-ray diffraction, and dynamic viscoelastometer. It is observed that blends are incompatible in the 20–80% blend composition range. The two β-relaxation peaks each of PE and PP component appear in the dynamic spectra of these blends. The two peaks, however, merge into a very broad, single relaxation peak at lower blend compositions (9 and 18% blends), indicating reasonably good compatibility between the two blend components. Variation of PP and EP_bC content in blends with HDPE affects the melting and crystallization temperature, crystallinity, crystallite dimensions, and crystallite and amorphous phase orientation of blend components, which, in turn, affect the mechanical properties of drawn tapes. © 1996 John Wiley & Sons, Inc.

INTRODUCTION

Within the last decade propylene and ethylene multiphase polymer systems including polymer blends have assumed importance technologically and commercially. Blends of polyethylenes (PE), with polypropylene or various types of ethylene-propylene copolymers, have been investigated.[1–15] It shows that these blend systems are immiscible in nature and that the blend components crystallize independently. However, many research workers[4–7] have also reported a positive synergistic improvement in mechanical and end-use properties for some blend compositions. The reason for the synergism has been qualitatively ascribed to the composition-dependent partial miscibility of PE/PP molecular chains in the molten state, change in crystallization kinetics, and the resultant morphology of blends.[2] In recent years, therefore, several studies have been undertaken to investigate the effect of molecular characteristics, blend composition, dispersion level, and melt miscibility on crystallization behavior, gross morphology, interfacial adhesion, plastic deformation behavior, and properties of PE/PP blends.[1–15]

As a part of the continuing effort to study structure–property relationships of high-density polyethylene (HDPE)/PP and HDPE/ethylene–propylene block copolymer (EP_bC) blends, we carried out a detailed investigation of the structure–morphology and its relationship to physical, mechanical, and thermal properties of these blends. The influence of blending, in terms of the type of blend components and blend composition, on deformation behavior of undrawn tapes and the structure–morphology, including crystallite and amorphous phase orientation of drawn blended tapes, is also explored.

EXPERIMENTAL

Materials and Sample Preparation

The commercial polymer grades used in this study are listed in Table I, together with the values of melt flow index (MFI). The PE/PP blend is known to be

* To whom correspondence should be addressed.

Journal of Applied Polymer Science, Vol. 60, 1527–1538 (1996)
 CCC 0021-8995/96/101527-12

Table I Material Characteristics

Polymer Type	Commercial Code	Supplier	MFI	Density (g/cm^3)	Comonomer Type and Composition
HDPE	GF 7745F	PIL, India	0.7*	0.945	1.8 CH_3/100C
PP	S-3030	IPCL, India	3.0	0.910	—
EP_bC	MI-3530	IPCL, India	3.5	0.900	6.8 mol % ethylene

* MFI measured at 190°C.

incompatible and so to produce as coherent a blend as possible, grades of HDPE, PP, and EP_bC of similar MFI were used.[10] As-received HDPE sample was characterized by ^{13}C-NMR spectroscopy for branch content. The details of this characterization are given elsewhere.[16] The ethylene and propylene composition of ethylene-propylene block copolymer was analyzed by IR spectroscopy. The IR spectrums recorded in the range of 700–900 cm^{-1} were analyzed using literature band assignments.[17]

Drawn blended tapes of blend composition, 100/0, 91/9, 82/18, 50/50, 20/80, and 0/100 of HDPE/PP and HDPE/EP_bC were prepared using a Betol-1820, single screw extruder of L/D ratio 20, with a slit die having width and thickness dimensions of 13 and 0.4 mm, respectively. The temperature profile used for extrusion was 160°C at the feed zone, 200°C at the compression zone, and 220°C at the metering zone and the die end. The screw speed was kept at 12 rpm. The extruded tapes were immediately quenched in a water bath maintained at 30°C and subsequently were drawn on a 750-mm-long hot plate maintained at 95°C with a draw ratio of 10×. After drawing, the drawn tapes were collected on a take-up bobbin with a velocity of about 10 m/min. The drawn tapes averaged between 950 and 1000 denier (denier is the weight in grams of 9000 meters of tape).

For study of undrawn tapes, the as-extruded tapes were collected after quenching in water on a take-up bobbin with a velocity of about 1 m/min.

Characterization of Undrawn and Drawn Tape

Density and Degree of Crystallinity

The density of undrawn tapes was measured on a Davenport density gradient column. The weight fraction crystallinity $X_{c(den)}$ was determined using crystalline and amorphous densities for HDPE and PP as 1.004, 0.853, and 0.946, 0.853 g/cm^3, respectively.[18] For blends of HDPE/PP and HDPE/EP_bC, the crystallinity was obtained using a relationship proposed by Wlochowicz and Jeziorny.[19]

Differential Scanning Calorimetry

Thermal behavior was followed through differential scanning calorimetry (DSC) measurements on a Perkin–Elmer DSC-7. Measurements were made with 8-mg samples in temperature range between 30 and 180°C at a scanning rate of 20°C/min. The crystalline weight fraction of polyethylene [$X_{c(PE)}$] and polypropylene [$X_{c(PP)}$] blend components was determined using standard heat of fusion as 293 and 163 J/g for HDPE and PP, respectively.[18] The maximum lamellae size in chain direction [$L_{c(dsc)}$] for each blend component was estimated using Thomson equation as applied to polyethylene and polypropylene by Wlochowicz and Eder.[20]

Birefringence

Birefringence (Δn) of drawn tapes was measured on a Leitz (Laborlux-12 POL) polarizing microscope fitted with a Leitz–Wetzler tilting plate-type compensator.

Wide-Angle X-ray Diffraction

Wide-angle X-ray diffraction (WAXD) studies were carried out for determination of average lateral crystallite size (D_{hkl}) and crystallite orientation factor (f_c), for drawn tapes. A Philips X-ray generator equipped with a Philips fiber goniometer was used for this study. The average lateral crystallite thicknesses were estimated from the broadening observed in WAXD patterns of powder samples using the Scherrer equation.[21] The shape factor (K) of the Scherrer equation has been shown by Hindeleh and Johnson[22] to vary considerably depending on crystallite shape, lattice distortion, and the reflection being studied. In absence of any further information and because crystallite shape in blend systems are very ill-defined, a value of unity was chosen. The crystallite orientation factor was estimated from azimuthal intensity distributions of (200) and (020) reflections for polyethylene[21] and (110) and (040) reflections for polypropylene crystallites.[21,23] It is

assumed that the recorded diffraction patterns of each crystallographic plane in the azimuthal scan is free from other diffraction interference.

Amorphous Orientation Factor

Birefringence was used to determine the amorphous orientation factor (f_{am}). The birefringence of a blend sample is the sum of crystalline and amorphous contributions of each blend component and depends on X_c, f_c, f_{am}, and intrinsic birefringence of crystalline ($\mathring{\Delta}n_c$) and amorphous ($\mathring{\Delta}n_{am}$) phases of blend components.

Equation (1) is used to compute average amorphous orientation function [$f_{am(avg)}$], of composite amorphous phase containing both PE and PP molecular chains.

$$\Delta n = \phi_1 X_{c1} f_{c1} \mathring{\Delta}n_{c1} + \phi_2 X_{c2} f_{c2} \mathring{\Delta}n_{c2} + (1 - X_c)_{avg} f_{am(avg)} \mathring{\Delta}n_{am(avg)} + \Delta f \quad (1)$$

where ϕ_i is the weight fractions of blend components and subscripts 1 and 2 refer to the components 1 and 2 of the blend system, respectively (see Table II). $[(1 - X_c)_{avg}]$ is the total noncrystalline weight fraction of blended sample and was estimated using the following equation:

$$(1 - X_c)_{avg} = [(1 - X_{c1})\phi_1 + (1 - X_{c2})\phi_2] \quad (2)$$

$[f_{am(avg)}]$ is the average orientation factor of a composite amorphous phase. $[\mathring{\Delta}n_{am(avg)}]$ is the weight average intrinsic birefringence of the composite amorphous phase containing blend components 1 and 2. The values of $\mathring{\Delta}n_{am(avg)}$ used in eq. (1) for various blend compositions were obtained from eq. (3).

$$\mathring{\Delta}n_{am(avg)} = \frac{(1 - X_{c1})\phi_1 \mathring{\Delta}n_{am1} + (1 - X_{c2})\phi_2 \mathring{\Delta}n_{am2}}{(1 - X_{c1})\phi_1 + (1 - X_{c2})\phi_2} \quad (3)$$

Equation (3) assumes that there are, in all, three phases in the fibrous structure, viz. crystallized fraction of 1, 2, and a intimately mixed composite amorphous phase, containing molecules of both blend components, which follows a simple additivity rule for estimation of $\mathring{\Delta}n_{am(avg)}$.

The values of $\mathring{\Delta}n_c$ and $\mathring{\Delta}n_{am}$ taken for analysis are 0.057 and 0.043 in the case of polyethylene[24] and 0.0291 and 0.060 for polypropylene,[23] respectively. Form birefringence (Δf) is neglected in this calculation; its value is certainly small in the case of partially miscible blends[25] but increases upon phase segregation.

Small-Angle X-ray Scattering

Small-angle X-ray scattering (SAXS) patterns were obtained on a set-up comprising a rotating anode X-ray generator operating at 50 KV and 200 mA and fitted with a Rigaku–Europe, compact small-angle goniometer, which defined the X-ray beam (nickel filtered CuK_α radiation). The raw scattering data is corrected for slit smearing using Schmidt and Height method.[26] The desmeared intensities were then Lorentz factor corrected.[21] The long period (L_p) is estimated by applying Bragg's law to the scattering angle of the maximum intensity measured parallel to the tape axis. The lamellae size in chain direction [$L_{c(SAXS)}$] is obtained by multiplying L_p with fraction of density crystallinity.

Table II Weight Fractions of Polyethylene and Polypropylene Components for HDPE/PP and HDPE/EP$_b$C Blends

% Blend Composition	HDPE/PP Blends Sample Code	ϕ_1 PE	ϕ_2 PP	HDPE/EP$_b$C Blends Sample Code	ϕ_1 PE	ϕ_2 PP
0	HDPE (control)	1.00	0.00	HDPE (control)	1.00	0.00
9	9 PP	0.91	0.09	9 EP$_b$C	0.92	0.08
18	18 PP	0.82	0.18	18 EP$_b$C	0.83	0.17
50	50 PP	0.50	0.50	50 EP$_b$C	0.53	0.47
80	80 PP	0.20	0.80	80 EP$_b$C	0.26	0.74
100	100 PP	0.00	1.00	100 EP$_b$C	0.07	0.93

Table III Density Crystallinity, DSC Crystallinity, Lamellae Size, and DSC Crystallization Data of Undrawn Tapes

Sample	$X_{c(den)}$ (%)	$X_{c(dsc)}$ (%)		$L_{c(SAXS)}$ (Å)	$L_{c(dsc)}$ (Å)		T_{onset} (°C)	T_c (°C)
		PE	PP		PE	PP		
HDPE (control)	63	61	—	118	110	—	119.8	117.9
9 PP	59	60	29	103	98	74	118.0	116.6
9 EP_bC	56	55	18	81	72	51	118.0	116.0

Mechanical Properties

Drawing behavior of undrawn tapes was analyzed on an Instron tensile tester with a constant strain rate of 1000% min^{-1}, whereas for drawn tapes a strain rate of 100% min^{-1} and a gauge length of 150 mm was used.

The dynamic mechanical thermal analysis of drawn tapes was carried out in a tensile mode, using Rheovibron DVV II-EP dynamic viscoelastometer. All measurements were carried out at 3.5 Hz frequency as a function of temperature from −130 to +130°C with a heating rate of 3°C/min.

Thermal Shrinkage

A Perkin–Elmer thermomechanical analyzer (TMA) system was used to study the shrinkage behavior of drawn tapes. Measurements were made on 11-mm samples in the temperature range 30–130°C at a scanning rate of 20°C/min.

RESULTS AND DISCUSSION

Structure and Properties of Undrawn Tapes

Crystallization Behavior and Morphology

The data on crystallinity, lamellae size, temperature of onset of crystallization (T_{onset}), and peak crystallization temperature (T_c) of undrawn tapes of 9% blend composition is given in Table III. It is seen that the rate of crystallization of blends reduces as indicated by a decrease in T_{onset} and T_c of blends. In general, the degree of crystallinity and lamellae size decrease by blending PP and EP_bC with HDPE. Specifically, the degree of crystallinity derived from density measurements is reduced from 63% for HDPE homopolymer to 59 and 56% for 9 PP and 9 EP_bC blends, respectively. The DSC crystallinity measured from the heat of fusion of individual blend components shows similar results. The 9 PP blend shows PP crystallinity of 29%, while only 18% PP component of 9 EP_bC blend is able to crystallize in case of 9 EP_bC blend. These results are consistent with the observed reduction in average lamellae size of these blends.

The HDPE lamellae size derived from SAXS experiments shows a decrease from 118 Å to about 103 and 81 Å for 9 PP and 9 EP_bC blends, respectively. Maximum lamellae size of each blend component was obtained from DSC endothermic peaks using Thomson equation.[20] These results are given in Table III and compare well with SAXS results. It is seen that lamellae of PP component are bigger in 9 PP than in 9 EP_bC blend specimen. The reduction in lamellae size of PP component of 9 EP_bC blend specimen is attributed to (a) partial miscibility of blend components in the melt state, leading to higher molecular entanglement density and (b) the limited number of sufficiently long crystallizable PP segments in EP_bC available for crystallization.

Drawing Behavior

The nominal stress–strain curves of HDPE homopolymer and blends are shown in Figure 1. The results indicate a marginal drop in yield stress (σ_y) on blending. The σ_y decreased from 21 MPa for HDPE homopolymer tapes to 14 MPa and 16 MPa for 9 PP and 9 EP_bC, respectively. These results are consistent with the observed reduction in degree of

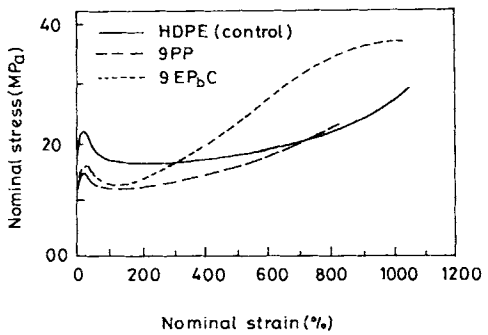

Figure 1 Nominal stress–strain curves of undrawn tapes of HDPE and its blends.

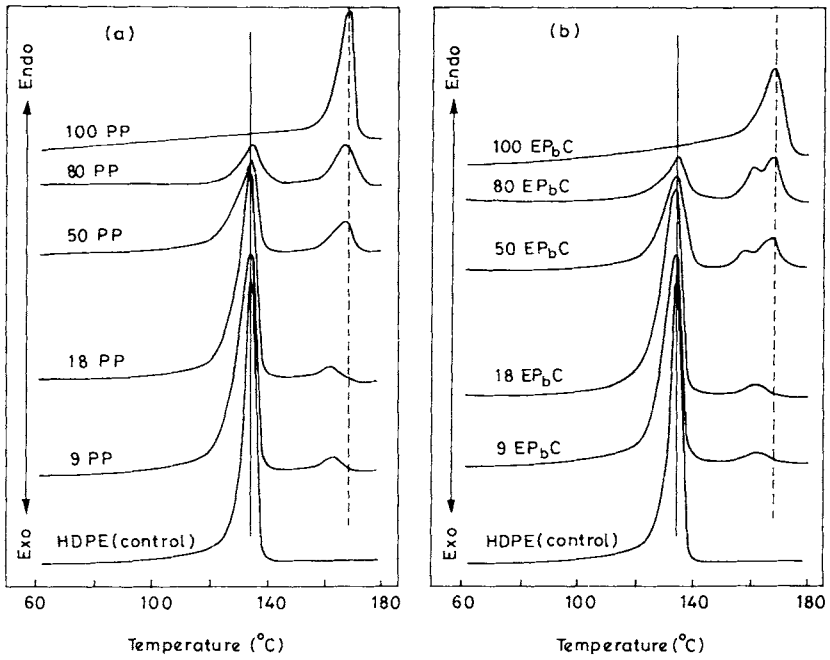

Figure 2 DSC melting exotherms of (a) HDPE/PP and (b) HDPE/EP_bC blends.

crystallinity and lamellae size that are known to exhibit a weaker resistance to onset of plastic deformation. Similar reductions in σ_y with decreasing crystalline fraction and lamellae size have been reported by several authors.[27-30]

In contrast to yield stress, the nominal tensile stress at higher strains is much higher for 9 EP_bC blend compared with HDPE. The natural draw ratio of this blend is also reduced significantly. It is, therefore, attractive to speculate that reduced the natural draw ratio and enhanced strain-hardening effect observed for HDPE/EP_bC blend might relate to the presence of a pseudo–rubber-like network in the amorphous phase that would increase the drawing stress required for molecular flow and its orientation. There are many evidences that support this phenomenon.[27-32]

The situation, however, is completely different for the HDPE/PP blend system. The marginal drop in σ_y, lower degree of strain hardening, and early failure of the specimen is associated with the poor melt miscibility, phase separation of blend components, and lower interphase adhesion. The reduction in σ_y can, therefore, be related to the reduction in mechanical connections between the lamellae of blend components. The decrease of the maximum achievable draw ratio and strain-hardening effect may come from the combined effect of interfacial slippage and failure at relatively weaker interphase boundaries.

Structure and Properties of Drawn Tapes

Melting and Crystallization Behavior

Figure 2 shows the melting endotherms of HDPE, PP, EP_bC, and their blends. The blends exhibit two melting peaks corresponding to PE and PP crystalline phases consistent with the reported literature.[12,33,34]

The peak melting temperature (T_m) of PE and PP components of blends are plotted against blend composition in Figure 3. The depression in melting temperature of one polymer associated with the presence of other component is seen. Such melting temperature depression in blends is well documented. A few selected polymer blend examples are poly(ethylene terephthalate) and poly(butylene terephthalate),[35] and poly(vinyl chloride) and poly-E-caprolactum.[36] In the present context, the depression in T_m of PP component for 9 and 18% compositions may relate to (i) partial melt miscibility of blend components and (ii) smaller and less perfect crystals. For 50 and 80% blends, the relatively small changes in T_m of blend components compared with the corresponding homopolymer are attributed to the complete phase segregation and formation of relatively bigger crystals.

Multiple endothermic peaks for PP are observed for 50 EP_bC and 80 EP_bC blends. The thermograms of these blends are shown in Figure 2(b). The minor peak observed at lower temperatures for PP crys-

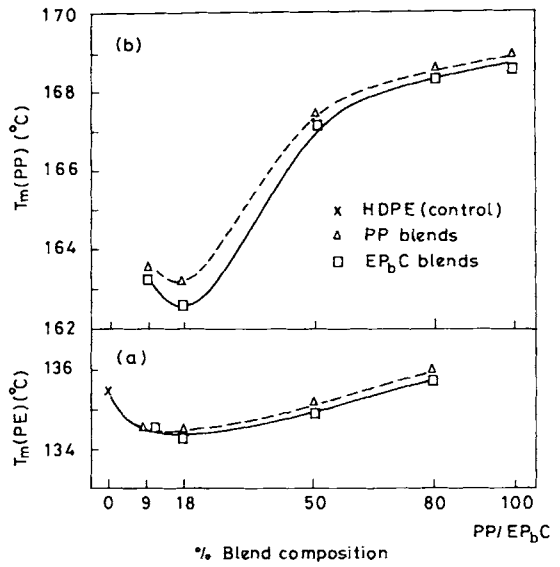

Figure 3 Peak melting temperature of (a) PE and (b) PP components of the blends as a function of blend composition.

talline fraction of HDPE/EP_bC blends indicates the presence of a significant amount of smaller and thermally less stable PP crystallites formed because of restrictions imposed by the ethylene segments of EP_bC for crystallization of PP segments.

In Figure 4 peak crystallization temperature (T_c) is plotted against blend composition. It follows from Figure 4 that for blends, the components crystallize almost simultaneously and show a single crystallization peak except at the 50% blend composition. The shift in composite peak crystallization temperature of 9 and 18% blends toward higher temperatures can be attributed to early nuclei formation of the PE component and hastened crystallization of PP. For 50% composition, two overlapping peaks are observed for both HDPE/PP and HDPE/EP_bC blends, indicating a distinct phase separation of blend components in the melt state.[2,37] At the 80% blend composition, however, again a single composite crystallization peak is observed. The significant lowering of composite peak crystallization temperature of these blends is related to the occlusion of the polyethylene component in the polypropylene matrix. Hence, in this case the PE component can not act effectively as the heterogeneous nuclei for crystallization of PP component. The crystallization process is, therefore, spread over a broader temperature range and the composite peak crystallization temperature of these blends is shifted to lower temperatures.

Crystallinity and Crystal Size

Crystallinity of each component has been estimated from the area under DSC endothermic peaks. Any changes during heating cycle in DSC are neglected. Figure 5 shows the relationship of $X_{c\,(PE)}$ and $X_{c\,(PP)}$ with blend composition for the two blend systems examined. From Figure 5(a) it follows that the addition of a small quantity of second-blend component to HDPE significantly reduces the crystallinity of the PE component. This effect is more pronounced for HDPE/EP_bC blends than HDPE/PP blends. At higher blend compositions, however, comparable PE crystallinity values are obtained and there is no significant difference between the crystallinity of HDPE homopolymer and $X_{c\,(PE)}$ of 50 and 80% blends, indicating phase segregation of components.

Figure 5(b) shows the dependence of $X_{c\,(PP)}$ on blend composition. The plots indicate a drastic drop in $X_{c(PP)}$ for 9 and 18% blends. This is in accordance with the results obtained for $X_{c(PE)}$ at similar blend compositions and is related to partial miscibility of blend components in the melt state and the associated decrease in overall molecular mobility. At higher percentage of compositions, the drop in $X_{c(PP)}$ is a result of phase separation. This is indicated by the two separate crystallization exotherms among

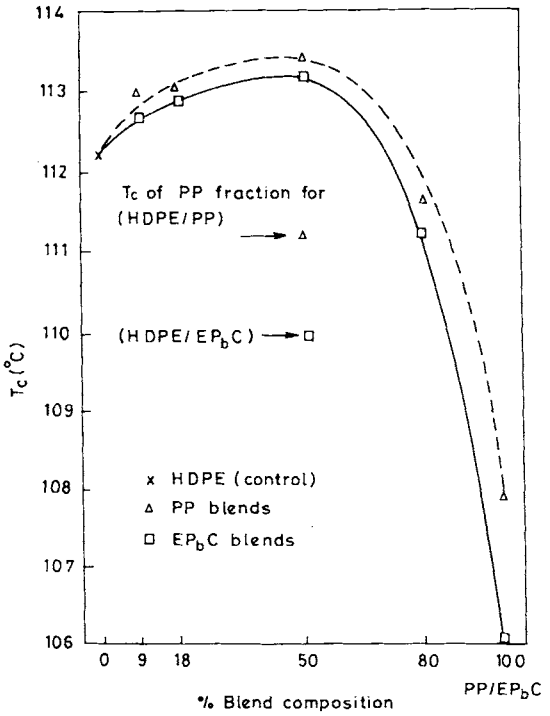

Figure 4 Peak crystallization temperature of blends as a function of blend composition.

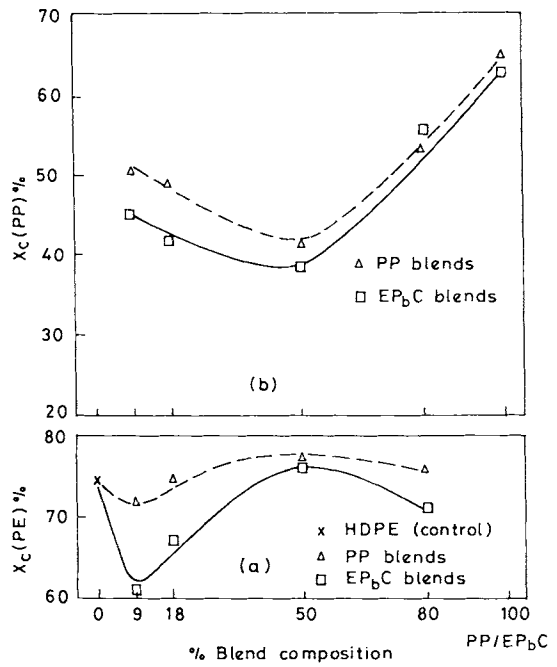

Figure 5 DSC crystalline fraction of (a) PE and (b) PP components of the blends as a function of blend composition.

which the PE component crystallizes first.[2,37] The crystallization of the PP component therefore takes place at higher melt viscosity of the system and thus decrease the molecular mobility and final crystallinity of the PP component.

Figures 6 and 7 show the WAXD patterns of various drawn tapes. It can be seen that WAXD patterns for blends are equivalent to a superposition of two individual homopolymer WAXD patterns. However, there is a enhanced (040) plane intensity of monoclinic polypropylene crystallites for 100 EP_bC specimens. Intensification of the diffraction of (040) plane is a result of the favored growth of PP crystallites in (040) direction than (110) direction. The quantitative data on crystal size obtained from WAXD patterns also support this fact (Fig. 8).

Figure 8 shows the dependence of lateral crystallite sizes of PE (D_{200} and D_{020}) and PP (D_{110} and D_{040}) on blend composition. Blending of polypropylene or ethylene-propylene copolymer into HDPE matrix reduces the size of polyethylene crystallites. The effect is more pronounced for 9% blends for which about 15% reduction in polyethylene D_{200} and D_{020} crystal size is observed. As stated earlier, these effects are associated with the decreased mobility of polyethylene molecules owing to its large-scale interactions with polypropylene or copolymer molecules in the melt and during crystal growth process. In contrast, at higher blend compositions the fractionation of blend components in the melt phase and subsequent crystallization of each blend components in their own melt phase results in crystals of bigger size.

Crystallite and Amorphous Phase Orientation

The crystallite orientation factors, $f_{c(PE)}$ and $f_{c(PP)}$ along with the orientation factor of a composite amorphous phase [$f_{am(avg)}$] for various blends are plotted as a function of blend composition in Figure 9. It is seen that the crystallite orientation factors of PE and PP components of the drawn blended tapes significantly decrease with the addition of a small amount of second-blend component and approaches an equilibrium value for blends at about 20 and 80% blend composition, respectively.

On the contrary, the results obtained for $f_{am(avg)}$ show a marginal increase in amorphous phase orientation at 9 and 18% composition. Higher $f_{am(avg)}$ of these blends is related to (a) partial miscibility of blend components in the amorphous phase, (b) lower crystallinity and smaller crystals, and (c) better interphase adhesion of two blend compo-

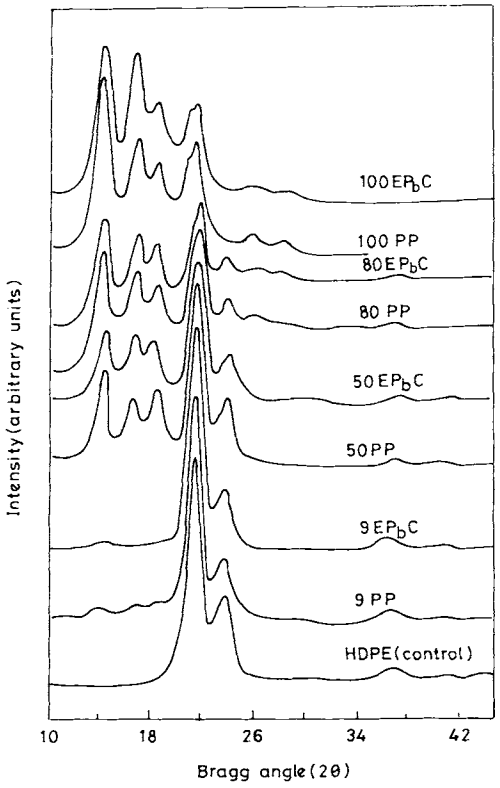

Figure 6 X-ray diffractograms of polyblends.

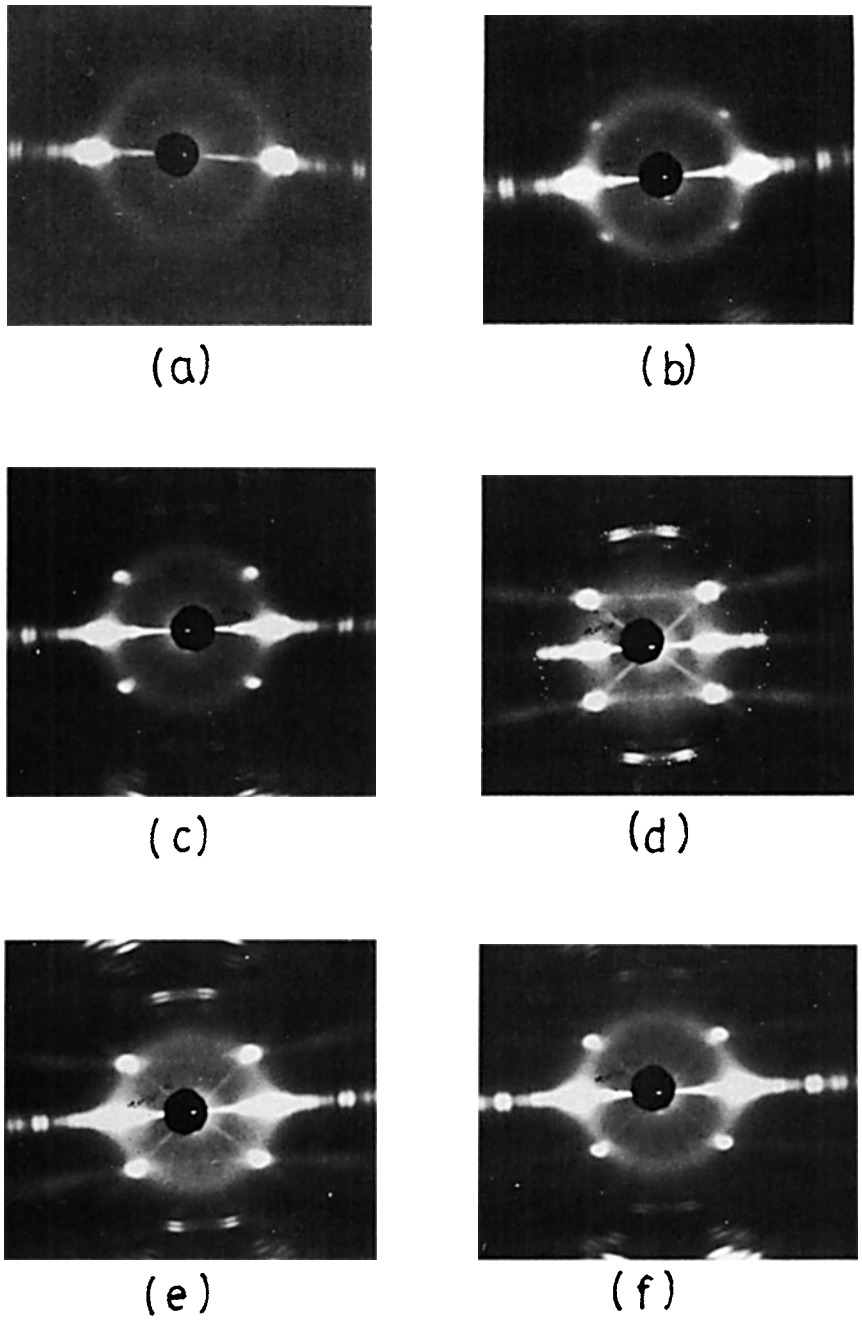

Figure 7 Wide-angle X-ray diffraction photographic patterns of (a) HDPE, (b) 9 PP, (c) 18 PP, (d) 50 PP, (e) 80 PP, and (f) 100 PP.

nents through interconnected–intercrystalline network structure. During deformation, the two interconnected species may, therefore, respond to the drawing stress more effectively with the formation of a large number of micronecks in the primary neck region and subsequently by the easy chain unfolding of the lamellae. At higher blend compositions, i.e., beyond 18% composition, however, the drawn blended tapes exhibit a drastic reduction in $f_{am(avg)}$. This is true, specifically, for immiscible blend systems where low attractive or adhesive forces between the two phases are to be expected. It is believed that this low degree of interfacial adhesion causes poor drawing stress transfer, leading to debonding and interfacial slippage at weaker interphase boundaries.

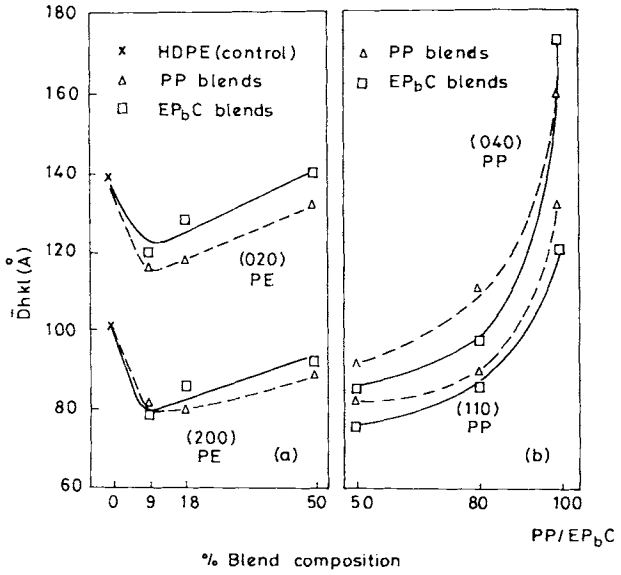

Figure 8 Lateral dimensions of PE and PP crystals as a function of blend composition.

Shrinkage Behavior

Figure 10 shows the effect of blend composition on shrinkage behavior of drawn tapes. The significant increase in shrinkage at 130°C manifests large-scale melting of small and thermally less stable PE crystals, a rapid increase in retractive stress, and the relaxation of oriented network structure.

The significantly higher shrinkage of 18% blends at 130°C compared with both HDPE homopolymer and 9% blends is related to the thermally less stable crystallites, higher amorphous phase orientation, and phase separation during the experiment. The latter effect may occur as a result of partial melting of smaller PE crystallites and subsequent relaxation of oriented molecular network, accompanied with the reorganization of structure. However, PP-rich blends, with a comparatively lower shrinkage tendency both at 110 and 130°C, clearly exhibit higher thermal stability of PP crystals and lower degree of amorphous phase orientation.

Mechanical Properties

In Figure 11 breaking stress (σ_b), breaking strain (ϵ_b), and initial modulus (E) are plotted against blend composition for various blend systems studied. Breaking stress and modulus vs. blend composition curves show synergism at 9 and 18% blend composition. The form of curves is very similar to that obtained by Deanin et al. for HDPE/PP,[6,38] LDPE/PP,[6] and LDPE/ethylene-propylene copolymers.[39]

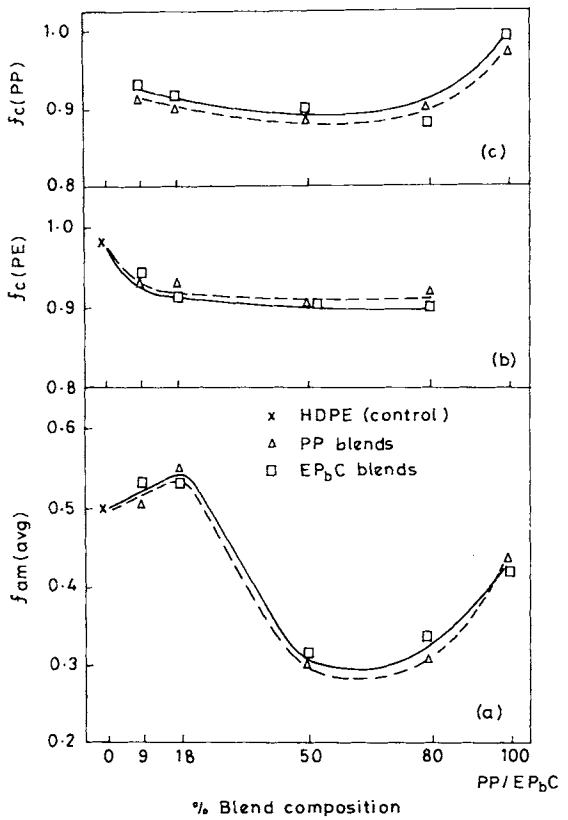

Figure 9 (a) Amorphous phase orientation factor, (b) crystallite orientation factor of polyethylene component, and (c) polypropylene component as a function of blend composition.

The increase in breaking stress and modulus at 9 and 18% blend composition is associated with the increased amorphous phase orientation. This, in turn, relates to the increased fraction of intercrys-

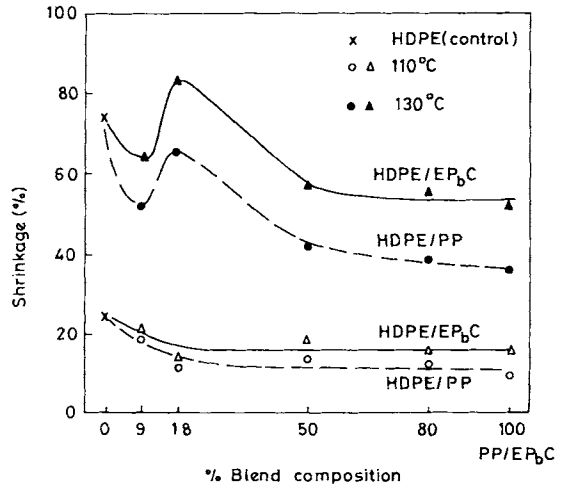

Figure 10 Variation of shrinkage as a function of blend composition.

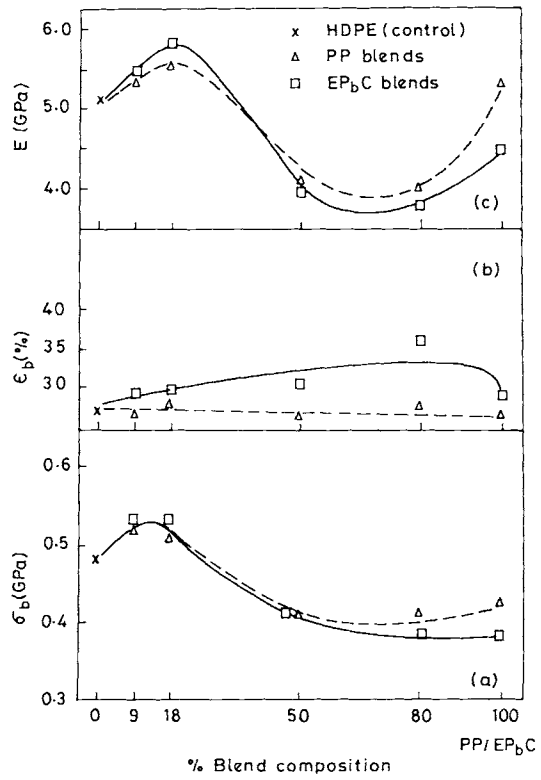

Figure 11 (a) Ultimate breaking stress, (b) breaking strain, and (c) initial modulus as a function of blend composition.

talline load-bearing taut-tie molecules. In contrast, the inferior mechanical properties at 50 and 80% blend compositions are the result of gross phase segregation of blend components, poor drawability, and lower amorphous phase orientation.

Figure 12 summarizes the key effects of blending on stress–strain behavior of drawn tapes of 9% blend composition. The important features are the markedly higher strain hardening, higher elongation to break, and greater energy to fracture for 9 EP_bC blends compared with 9 PP and HDPE homopolymer tapes. This is in agreement with the enhanced amorphous phase orientation and suggested increase in molecular network of 9 EP_bC blend.

Dynamic Mechanical Behavior

In Figure 13 the results on dynamic mechanical behavior in terms of loss tangent (tan δ) is represented as a function of temperature for HDPE/PP and HDPE/EP_bC blends of a few selected composition.

HDPE tapes show characteristic β-transition at $-114°C$, as well as, a broad transition between -35 and $-28°C$. Similar results are also obtained for 9% blends, indicating partial miscibility in amorphous phase and a reasonably good compatibility. The 18% blends also show a broader single β-relaxation peak in the vicinity of -23 and $-15°C$ for 18 PP and 18 EP_bC blends, respectively, suggesting that these blends are partially miscible and compatible. However, as shown earlier, these blends show phase segregation at higher temperatures, as indicated by the rapid increase in shrinkage behavior.

At higher blend compositions, two separate tan δ peaks of PE ($-30°C$) and PP ($-10°C$) components confirm phase segregation of blend components. These results are consistent with the earlier observations of morphology and mechanical behavior of tapes.

CONCLUSIONS

The effect of blending PP with HDPE and EP_bC with HDPE on structure, morphology, and properties of binary blends has been studied systematically. In general, these blends are heterogeneous in nature and no cocrystallization phenomenon was detected. The crystallization behavior, structure–morphology, and drawing behavior of HDPE is affected markedly by blending PP or EP_bC.

The drawn blended tapes of HDPE/PP and HDPE/EP_bC show incompatibility, especially in the range of 20 and 80% blend composition. In case of 9 and 18% compositions the compatible amorphous phase and interconnected intercrystalline molecular network is strong enough to result in blends having higher amorphous phase molecular orientation and improved mechanical properties. The comparatively lower degree of amorphous phase orientation and inferior mechanical properties at 50 and 80% blend composition are, however, the result of gross phase segregation of blend components, poor interphase adhesion, and debonding at weaker interphase

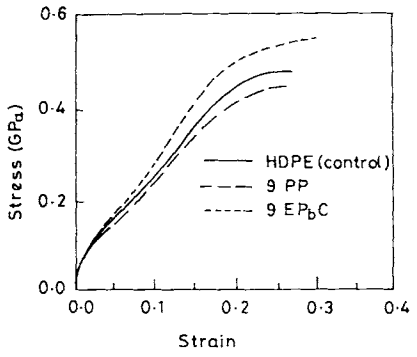

Figure 12 Stress–strain plots of drawn tapes of HDPE and its blends.

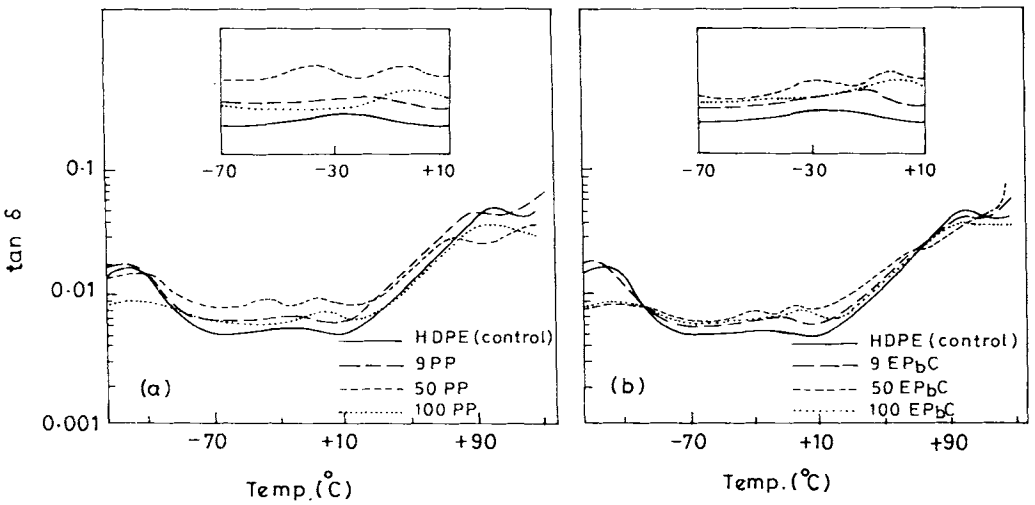

Figure 13 Temperature dependence of the loss tangent for drawn tapes.

boundaries during drawing. Dynamic mechanical behavior of these tapes support the phase behavior at different compositions.

REFERENCES

1. E. Martuscelli, M. Pracella, M. Avella, R. Greco, and G. Ragosta, in *Polymer Blends: Processing, Morphology and Properties,* Vol. 1, E. Martuscelli, R. Palumbo and M. Kryszewski, Eds., Plenum Press, New York, 1979, p. 49.
2. J. Grebowicz and T. Pakula, in *Polymer Blends: Processing, Morphology and Properties,* Vol. 1, E. Martuscelli, R. Palumbo and M. Kryszewski, Eds., Plenum Press, New York, 1979, p. 87.
3. J. W. Teh, *J. Appl. Polym. Sci.,* **28,** 605 (1983).
4. A. J. Lovinger and M. L. Williams, *J. Appl. Polym. Sci.,* **25,** 1703 (1980).
5. O. F. Noel and J. F. Carley, *Polym. Eng. Sci.,* **15,** 117 (1975).
6. R. D. Deanin and M. F. Sansone, *Polym. Prepr., Am. Chem. Soc. Div. Polym. Chem.,* **19**(1), 211 (1978).
7. R. Greco, G. Mucciariello, G. Ragosta, and E. Martuscelli, *J. Mater. Sci.,* **15,** 845 (1980).
8. R. Greco, G. Mucciariello, G. Ragosta, and E. Martuscelli, *J. Mater. Sci.,* **16,** 1001 (1981).
9. M. Tang, R. Greco, G. Ragosta, and S. Cimmino, *J. Mater. Sci.,* **18,** 1031 (1983).
10. S. Danesi, in *Polymer Blends: Processing, Morphology and Properties,* Vol. 2, E. Martuscelli, R. Palumbo and M. Kryszewski, Eds., Plenum Press, New York, 1979, p. 35.
11. P. Robson, G. J. Sandilands, and J. R. White, *J. Appl. Polym. Sci.,* **26,** 3515 (1981).
12. G. A. Gallagher, R. Jakeways, and I. M. Ward, *J. Appl. Polym. Sci.,* **43,** 1399 (1991).
13. S. Onogi, T. Asada, and A. Tanaka, *J. Polym. Sci.* A2, **7,** 171 (1969).
14. H. W. Kammer, G. Kummerloewe, R. Greco, C. Mancarella, and E. Martuscelli, *Polymer,* **29,** 963 (1988).
15. F. Coppola, R. Greco, E. Martuscelli, H. W. Kammer, and C. Kummerloewe, *Polymer,* **28,** 47 (1987).
16. S. K. Rana, *Crystallization Behaviour and Structure Property Correlation of High-Density Polyethylene/ Linear-Low Density Polyethylene Blends,* Ph.D. Thesis, Indian Institute of Technology, Delhi, July 1992.
17. Ser Van der Ven, *Polypropylene and Other Polyolefins—Polymerization and Characterization,* Elsevier, Amsterdam, 1990, p. 447, 535.
18. R. P. Runt, in *Encyclopedia of Polymer Science and Engineering,* Vol. 4, 2nd Ed., H. F. Mark, N. M. Bikales, C. G. Overberger and G. Menges, Eds., Wiley-Interscience, New York, 1986, p. 482.
19. A. Wlochowicz and A. Jeziorny, *J. Polym. Sci.,* **C30,** 399 (1970).
20. A. Wlochowicz and M. Eder, *Polymer,* **25,** 1268 (1984).
21. L. E. Alexander, *X-Ray Diffraction Methods in Polymer Science,* Krieger Press, New York, 1979.
22. A. M. Hindeleh and D. J. Johnson, *Polymer,* **19,** 27 (1978).
23. R. J. Samuels, *Structured Polymer Properties,* Wiley-Interscience, New York, 1974.
24. J. L. Pezzutti and R. S. Porter, *J. Appl. Polym. Sci.,* **30,** 4251 (1985).
25. D. Lefebvre, B. Jasse, and L. Monnerie, *Polymer,* **22,** 1616 (1981); ibid., **23,** 706 (1982); ibid., **25,** 318 (1984).
26. P. W. Schmidt and R. Height, Jr., *Acta Cryst.,* **17,** 138 (1960).
27. R. Seguela and F. Rietsch, *Eur. Polym. J.,* **20,** 765 (1984).

28. G. Capaccio and I. M. Ward, *J. Polym. Sci., Polym. Phys. Ed.*, **22,** 475 (1984).
29. G. Meinel and A. Peterlin, *Eur. Polym. J.*, **7,** 657 (1971).
30. G. Capaccio and I. M. Ward, *Polymer*, **16,** 239 (1975).
31. G. Capaccio, T. A. Crompton, and I. M. Ward, *J. Polym. Sci., Polym. Phys. Ed.*, **14,** 1641 (1976).
32. G. Capaccio, T. A. Crompton, and I. M. Ward, *J. Polym. Sci., Polym. Phys. Ed.*, **18,** 301 (1980).
33. E. Martuscelli, M. Pracella, G. Volpe, and R. Greco, *Makromol. Chem.*, **185,** 1041 (1984).
34. A. Galeski, Z. Bartczak, and M. Pracella, *Polymer*, **25,** 1323 (1984).
35. R. S. Stein, F. B. Khambatta, F. P. Warner, T. Rusell, A. Escala, and E. Balizer, *J. Polym. Sci., Polym. Symp.*, **63,** 313 (1978).
36. D. S. Hubbell and S. L. Cooper, *J. Appl. Polym. Sci.*, **21,** 3035 (1977).
37. M. Plesek and Z. Malac, in *Morphology of Polymers*, Blahoslav Sedlacek, Ed., Walter de Gruyter, Berlin, 1986, p. 347.
38. R. D. Deanin and G. E. D'Isidoro, *Org. Coatings and Plastics Chem.*, **43,** 19 (1980).
39. R. D. Deanin and S. T. Lim, *SPE ANTEC.*, **29,** 222 (1983).

Received June 16, 1994
Accepted October 7, 1995